MEASURING ROCKFALL AREA WITH SEASONAL NDVI

Yu-Chieh Huang[1,*] and Walter Chen[1]
[1]Department of Civil Engineering, National Taipei University of Technology
1 Sec 3 Chung-Hsiao E. Rd., Taipei 10608, Taiwan ROC
t109428125@ntut.org.tw, waltchen@ntut.edu.tw

Keywords: Rockfall, Rockslide, SPOT, NDVI

Abstract: Rockfalls and rockslides in Taiwan's hilly regions frequently block roads leading to remote villages, isolating residents from the outside world. Using the normalized difference vegetation index (NDVI) obtained from SPOT 6 and SPOT 7 satellite images, we examined a slope (hillside) with frequent rockfalls to quantify the rockfall frequency for the purpose of studying the hazard. The slope is located near the Yu-Feng Bridge in the Chien-Shih Township of Hsinchu County, Taiwan. We applied the criterion that rockfall locations on a slope are defined by NDVI values below a threshold (exposed rock surfaces). To eliminate the effect of seasonal variation of NDVI values, we determined the range of monthly NDVI values by calculating the NDVI values of a neighboring area with year-round vegetation cover. Then, each month, the slope areas with NDVI values lower than the corresponding NDVI threshold were designated as rockfall regions. This study examined images from 2019 to 2021 and discovered periodic changes in the rockfall/rockslide areas, indicating repetitive rockfall behavior.

1. INTRODUCTION

Rockfalls in Taiwan's hilly regions frequently block roads leading to remote villages, isolating residents from the outside world. They also cause considerable property damage and fatalities in Taiwan. This study aimed to examine a slope with frequent rockfalls/rockslides using remote sensing images to quantify the rockfall frequency for the purpose of studying the hazard.

In the past, the spatial resolution of satellite images was insufficient for small areas such as rockfall/rockslide slopes. For instance, SPOT 1 to SPOT 4 satellites provide 20 m resolution in multispectral bands and 10 m resolution in the panchromatic band, whereas SPOT 5 provides 10 m resolution in multispectral bands and 5 m resolution in the panchromatic band. These resolutions were inadequate for rockfall slope analysis. However, the SPOT 6 and SPOT 7 satellites offer 6 m multispectral and 1.5 m panchromatic resolutions. The high resolutions provide the opportunity to study rockfalls and produce desirable results.

Typical rockfall regions are characterized by the bare rock surface and the lack of surface vegetation. To identify the rockfall regions, we used the normalized difference vegetation index (NDVI), which could be calculated from SPOT 6/7 satellite images to indicate vegetation's presence and condition, to automatically identify rockfall locations on satellite images. The objective was to assess the size of rockfall/rockslide regions and track their periodic changes from 2019 to 2021.

2. LITERATURE REVIEW

NDVI is a widely used index in many research fields such as agriculture, forestry, landslide, and soil erosion analysis. As an illustration, Yang et al. (2019) determined the best thresholds for autonomously extracting landslide scars using NDVI computed from Sentinel-2 images. NDVI measurements from the Landsat-5 Thematic Mapper (TM) were used by Guerrero et al. (2016) to analyze seasonal variations in the NDVI values in slopes with a northerly or a southerly orientation. Tsai et al. (2013) constructed models for landslide detection using NDVI in data mining. Using NDVI time series data, Chao et al. (2011) investigated the temporal change of a mining subsidence area. In addition, Kocaaslan et al. (2021) evaluated drought occurrences on the Google Earth Engine (GEE) platform using NDVI obtained from the Moderate Resolution Imaging Spectroradiometer (MODIS) sensor. The NDVI from MODIS was also utilized by Quintano et al. (2010) to detect regions burned by forest fires. Finally, Tsai et al. (2021) constructed a machine learning model for multi-temporal soil erosion analysis using NDVI, and Gonzalez Loyarte and Menenti (2008) examined the effects of rainfall anomalies on vegetation phenology using monthly NDVI data spanning nine years. In each of the aforementioned examples, NDVI acted as a reliable measure of the existence and health of vegetation, as well as the accompanying changes. In this study, we selected the NDVI of a rock slope with a thin soil cover to differentiate rockfall/rockslide areas (nearly devoid of vegetation) from areas with normal vegetation.

3. MATERIAL AND METHODS

The study area is a hillside near the Yu-Feng Bridge in the Chien-Shih Township of Hsinchu County, Taiwan, which is adjacent to a major transportation route and near multiple communities. The slope is located in the coordinates 24°39'30" latitude and 121°18'30" longitude. Figure 1 shows a digital elevation model (DEM) of the Shihmen Reservoir watershed (top left), the Yu-Feng sub-watershed (bottom left), and an aerial photograph of the slope.

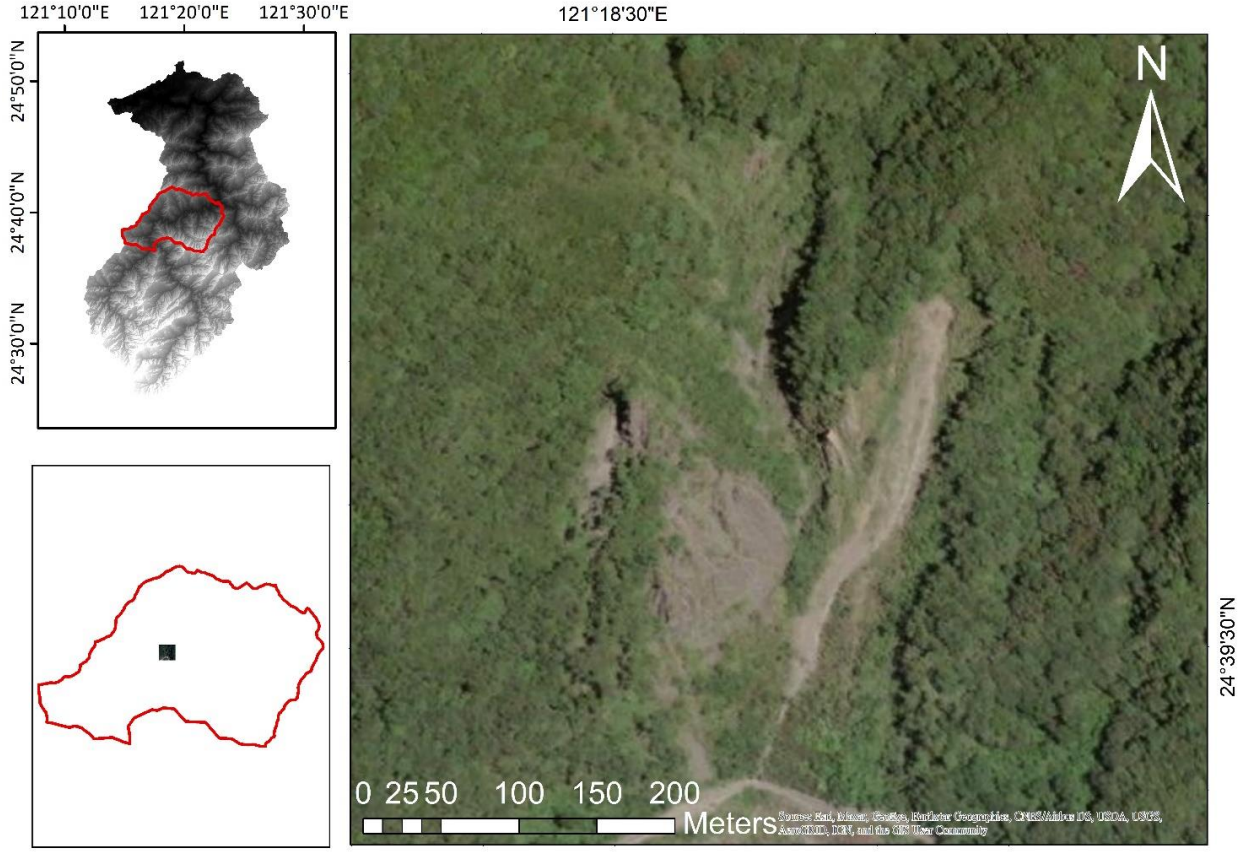

Figure 1 The geographical location of the study area (image source: ArcGIS base map)

Figure 2 depicts this study's flowchart. The primary objective was to use NDVI to automatically detect the rockfall area of a slope, taking into account the seasonal change of vegetation (vegetation phenology) and monitoring the area variation. NDVI is a standard way to measure vegetation health, and healthy vegetation reflects near-infrared (NIR) and green light. However, it absorbs more red and blue light. NDVI is calculated as follows:

$$NDVI = \frac{(\text{NIR} - \text{Red})}{(\text{NIR} + \text{Red})} \quad (1)$$

where
NIR: the near-infrared band of SPOT 6/7, which is band 4
Red: the red band of SPOT 6/7, which is band 3

The range of NDVI is between -1 and 1. The closer the number is to 1, the more likely it is dense green vegetation. As illustrated in Figure 2, we chose 36 monthly SPOT 6/7 images and converted each image's digital numbers (DN) to radiance and subsequently to top-of-atmosphere (TOA) reflectance. The TOA reflectance-based NDVI was computed for the reference area (green rectangle of Figure 3). Then, we applied a threshold of three standard deviations below the mean NDVI to calculate the size of the rockfall/rockslide region.

The images used in this study were obtained from the Center for Space and Remote Sensing Research (CSRSR) of the National Central University. According to Astrium Services (2013), the formulae for converting DN to radiance and TOA reflectance are as follows:

$$\mathrm{L_b}(p) = \frac{DC(p)}{\mathrm{GAIN(b)}} + \mathrm{BIAS}(b) \quad (2)$$

$$\rho_b\,(p) = \frac{\pi \cdot \mathrm{L_b}(p)}{E_0(b) \cdot cos(\theta_s)} \quad (3)$$

where
$L_b(p)$: top of atmosphere (TOA) radiance ($W \cdot sr^{-1} \cdot m^{-2} \cdot \mu m^{-1}$)
$DC(p)$: digital count of a pixel
$GAIN(b)$: radiometric calibration coefficient
$BIAS(b)$: radiometric calibration coefficient
$\rho_b\,(p)$: top of atmosphere (TOA) spectral reflectance
π: 3.1415926
$E_0(b)$: solar irradiance for SPOT 6/7
θ_s: $90 -$ solar elevation angle

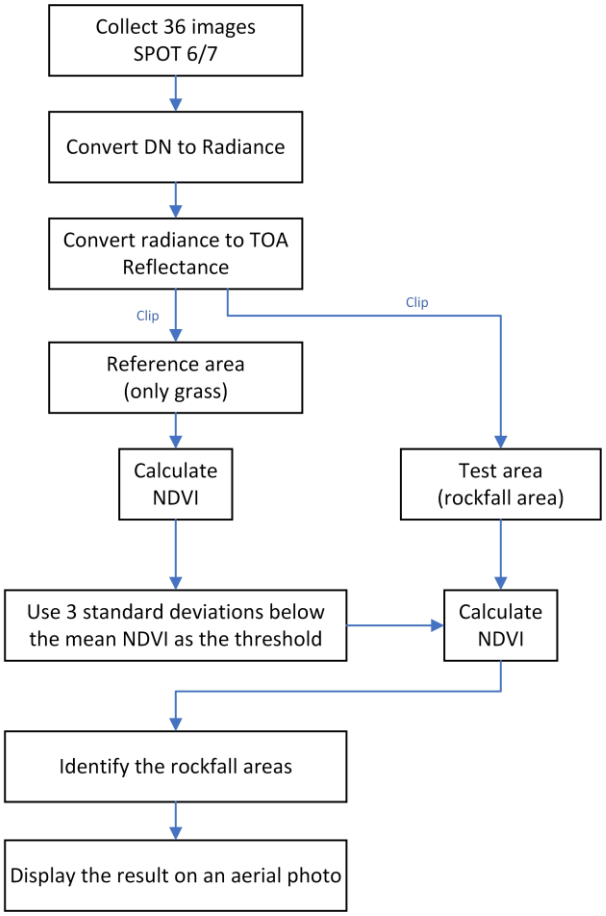

Figure 2 The research flow chart for this study

The reference area (green rectangle) and test area (dark brown polygon) are shown in Figure 3. The image is a composite of an ArcGIS base map (left) and an aerial photograph from the Aerial Survey Office of the Forestry Bureau, Taiwan (right). The reference area contains abundant green vegetation year-round and is close to places prone to rockfalls yet is not affected by them. Hence, the reference area was chosen to establish an NDVI benchmark value. The NDVI of the reference area fluctuates from month to month as a result of the phenology of the vegetation. We computed the mean and standard deviation of NDVI of the reference area. Assuming a normal distribution, 99.7% of the NDVI values should fall within ±3 standard deviations of the mean. Consequently, pixels with NDVI values below three standard deviations below the mean NDVI were designated as rockfall/rockslide regions. Every month's threshold NDVI value was different.

We counted the pixels and determined the size of the regions affected by rockfalls/rockslides. To observe the temporal change of NDVI at the study site, the same technique was employed for each of the 36 monthly images of SPOT 6/7 (6-m spatial resolution) across the span of 36 months (2019-2021).

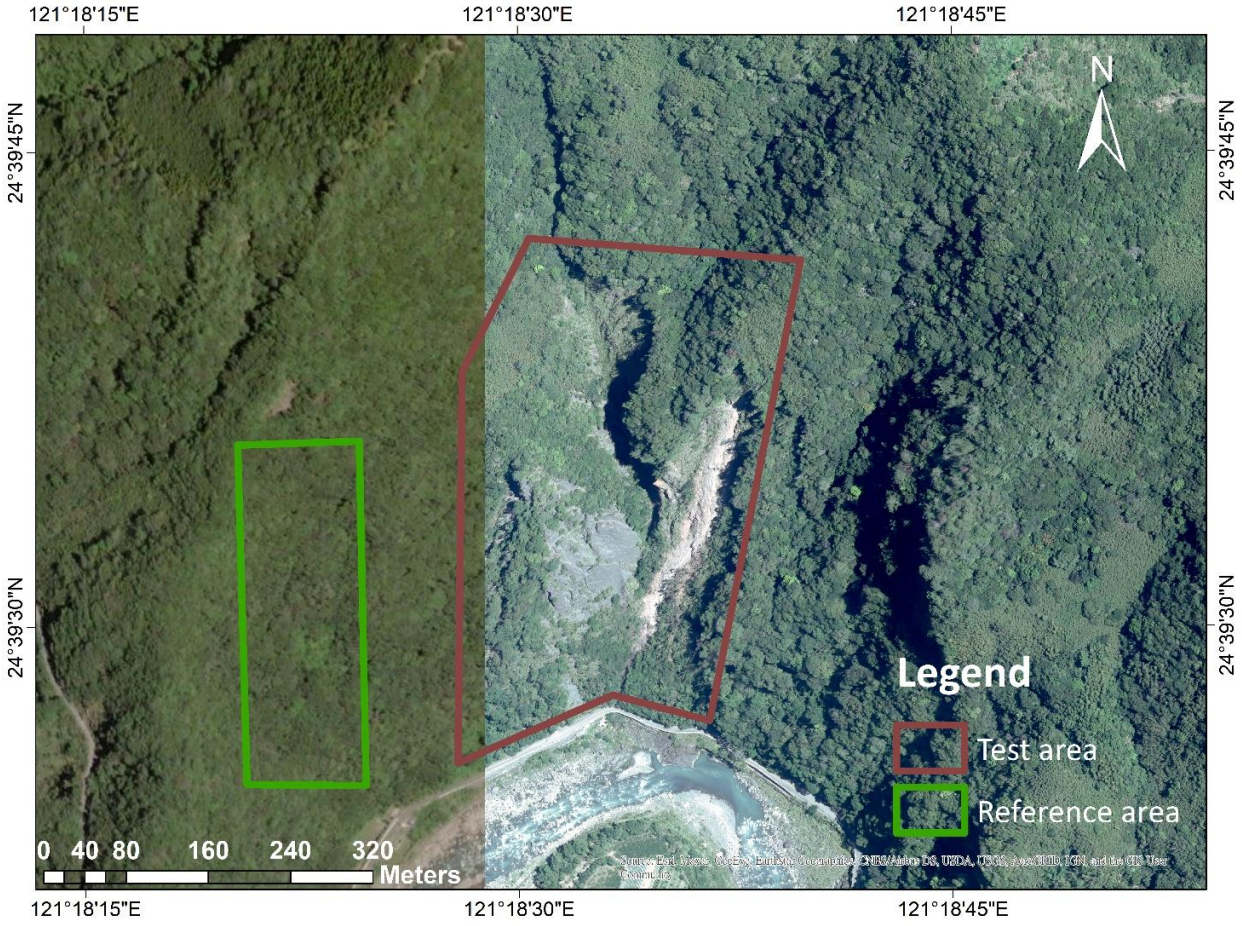

Figure 3 The reference area and test area on the slope near the Yu-Feng Bridge (image source: ArcGIS and Aerial Survey Office of the Forestry Bureau, Taiwan)

4. RESULTS

Figure 4 displays the research area's true color, false color, and NDVI images. The last image (bottom right) was an aerial photograph taken on June 17, 2021, whereas the other five images were based on the SPOT image of June 15, 2021. As illustrated in the left column, the original spatial resolution was 6 m (true color and false color). We used the Brovey transformation to create pan-sharpened images from the panchromatic and multispectral images, raising the spatial resolution to 1.5 m (middle column). Finally, as illustrated in the upper right image of Figure 4, the NDVI image was computed using equations (1) through (3). The bottom right image was a 0.25 m-resolution aerial photograph from the Aerial Survey Office of the Forestry Bureau, Taiwan.

One representative satellite image from each month from 2019 to 2021 was chosen and processed, similar to Figure 4. The mean and standard deviation of the reference area's NDVI values were calculated for each of the 36 images, and the results were summarized in Figure 5 (left column). It is clear that the mean NDVI varies on a monthly and seasonal basis. The beginning of each year always has the lowest mean NDVI values, and the mean NDVI values typically increase in the middle of the year and decline towards the end. However, the pattern of variation varies slightly from year to year. For 2019, 2020, and 2021, the increases in mean NDVI over a year were 32.7%, 35.2%, and 19.0%, respectively. Such a substantial variation in mean NDVI over a year demonstrates that selecting a fixed NDVI threshold for identifying rockfall regions is unreasonable.

Using three standard deviations below the mean NDVI as a threshold, we identified pixels with lower NDVI values as rockfall/rockslide regions. By doing so, the influence of vegetation phenology on the threshold value of NDVI from month to month was eliminated. To calculate the size of the rockfall regions on the slope for each month from 2019 to 2021, the pixels were added together and converted to square meters. The results are displayed in Figure 5's

right column. As depicted in Figure 5, the size of the rockfall regions did not stay the same and changed throughout time. The best explanation for these changes is the gradual regrowth of vegetation after rockfalls and rockslides removed it from the slope surface.

Figure 4 True color, false color, and NDVI images of the study area (June 15 and 17, 2021)

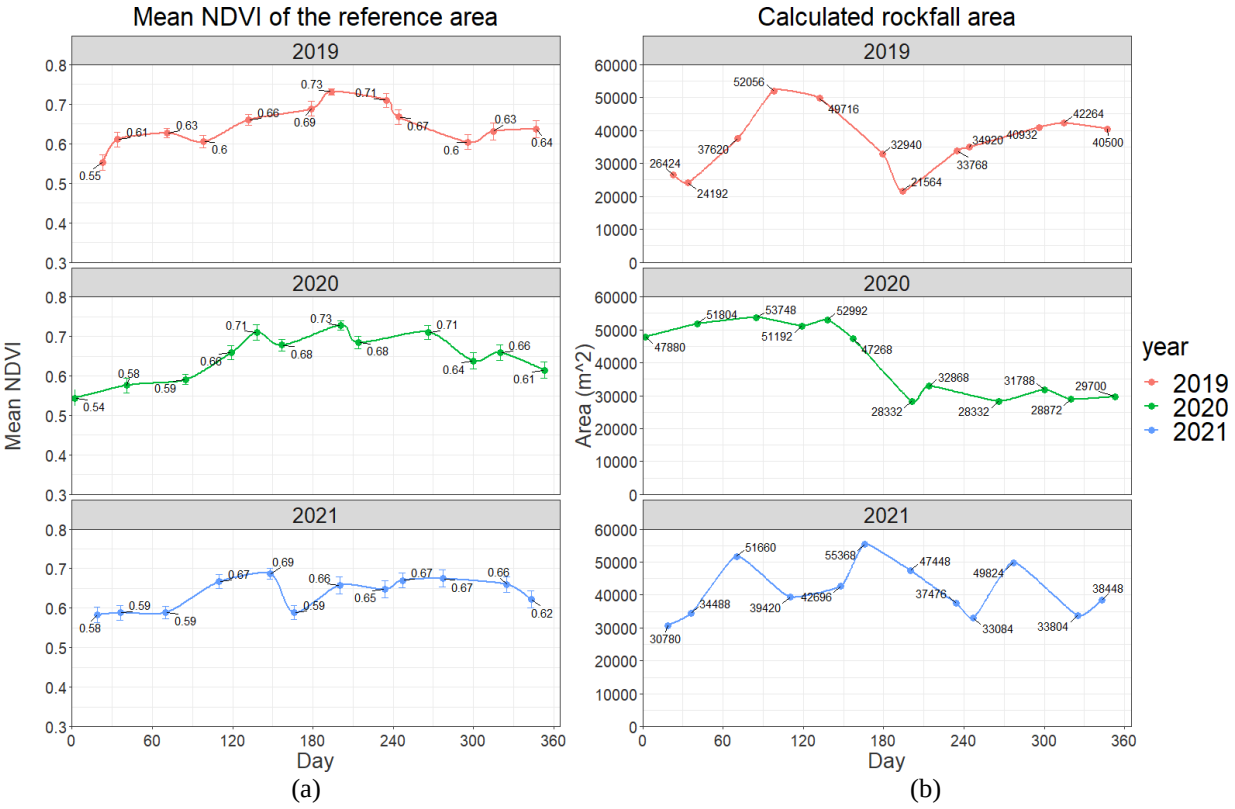

Figure 5 (a) The mean NDVI of the reference area from 2019 to 2021, and (b) the size of the rockfall regions from 2019 to 2021

There appeared to be two significant rockfall events in 2019 that repeatedly occurred over a period of several months (as indicated by the continuous increase in the area). During the first event, which occurred between February and

April, the rockfall area grew from 24192 to 52056 m^3. The second event occurred between July and November, during which time the rockfall area increased from 21564 to 42264 m^3. In 2020, there was a generally decreasing trend with small individual increases in the area, indicating a slow restoration of vegetation and the absence of a significant rockfall event. Finally, for the year 2021, there appeared to be three to four rockfall episodes, as suggested by three to four rises in the area. The rockfall area grew from 30780 to 51660 m^3 between January and March, 39420 to 55368 m^3 between April and June, 33084 to 49824 m^3 between September and October, and 33804 to 38448 m^3 between November and December.

Using 2021 as an example, we chose SPOT images corresponding to the first three increases in the rockfall area (six in total). As indicated in Figure 6, they were January to March, April to June, and September to October. We also superimposed red squares over image pixels to indicate NDVI values below the threshold. By studying the change in the pattern of the red squares, it is possible to determine where rockfalls may have occurred.

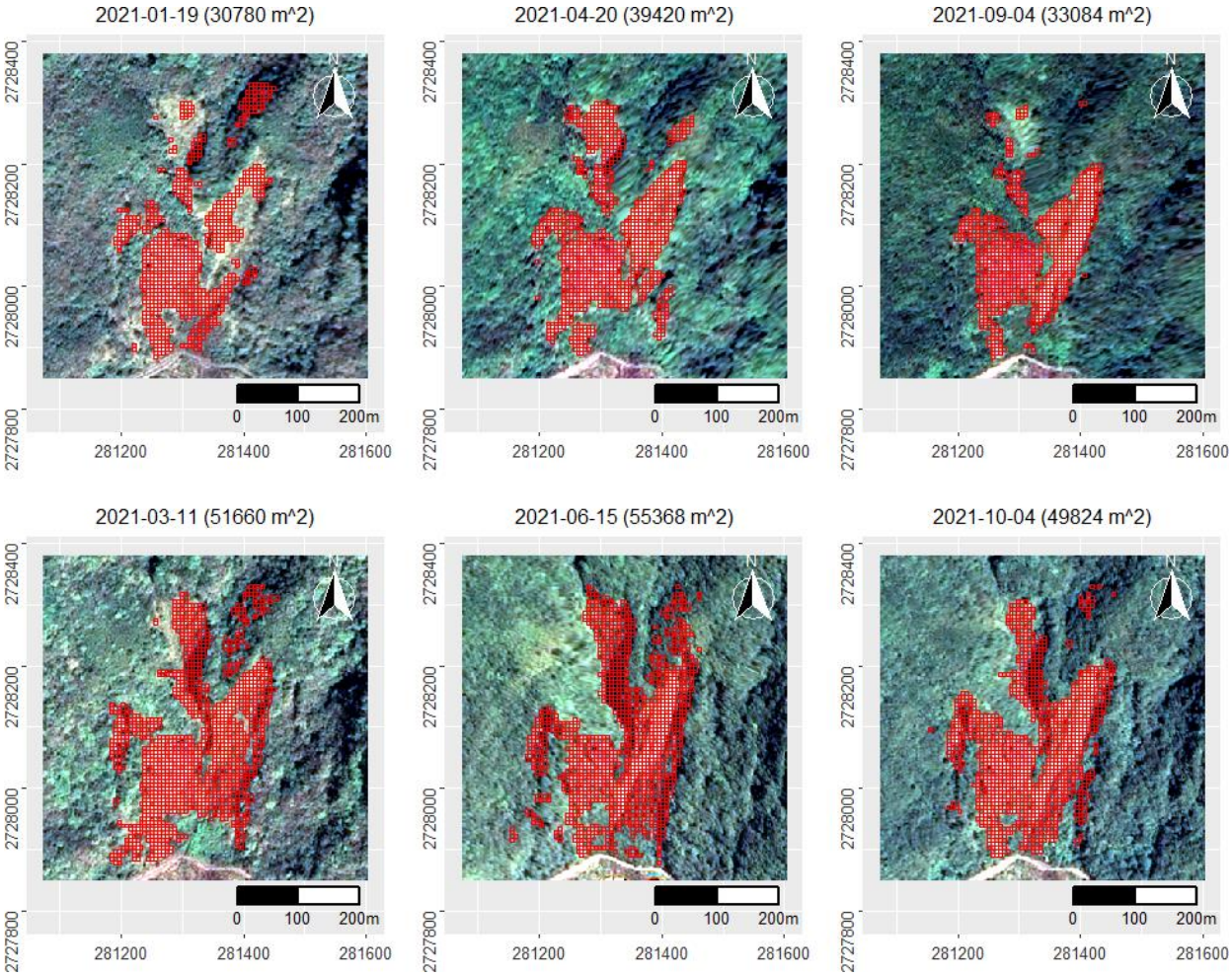

Figure 6 SPOT images of 2021 showing three possible rockfall events (January to March, April to June, and September to October)

5. DISCUSSION AND CONCLUSIONS

To determine the efficacy of our proposed method for identifying rockfall/rockslide regions, we compared the pan-sharpened June 15, 2021 SPOT image and the June 17, 2021 aerial photograph. This is illustrated in Figure 7. We also added red squares on the images to indicate the area identified as the rockfall/rockslide regions. In general, the red squares correspond nicely to the bare surface exposed by rockfalls and rockslides (low NDVI values). However, our suggested method also identified a few shadowy patches (caused by local depressions) as rockfall regions. This is a potential source of error. However, this inaccuracy can be overlooked if shadows appear consistently in images from other months, as we are only interested in the change in the size of the rockfall regions.

Figure 7 further reveals another issue: the red squares fit the SPOT image (left) better than the aerial photograph (right), despite the fact that the two images were captured only two days apart and were geometrically calibrated to the same coordinate system. The match between the red squares and the aerial photo was improved by rotating the

aerial photo slightly, as shown in Figure 8. This issue may be due to errors caused by the relief displacement in the study area, which is a mountainous area.

Last but not least, each pixel in this study's NDVI calculation was 6 m by 6 m in size. Consequently, it's likely that some pixels included a combination of vegetation and bare surface, which could skew the outcomes of the analysis slightly.

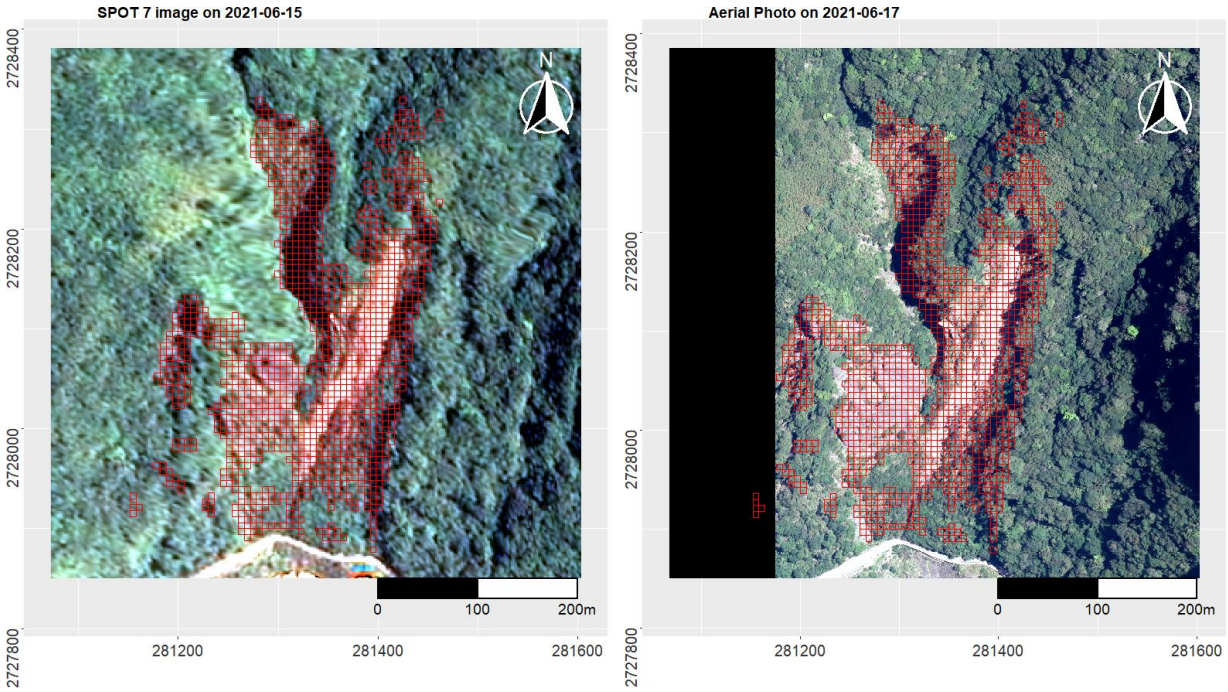

(a) (b)

Figure 7 (a) The pan-sharpened SPOT image taken on June 15, 2021, and (b) the aerial photo taken on June 17, 2021

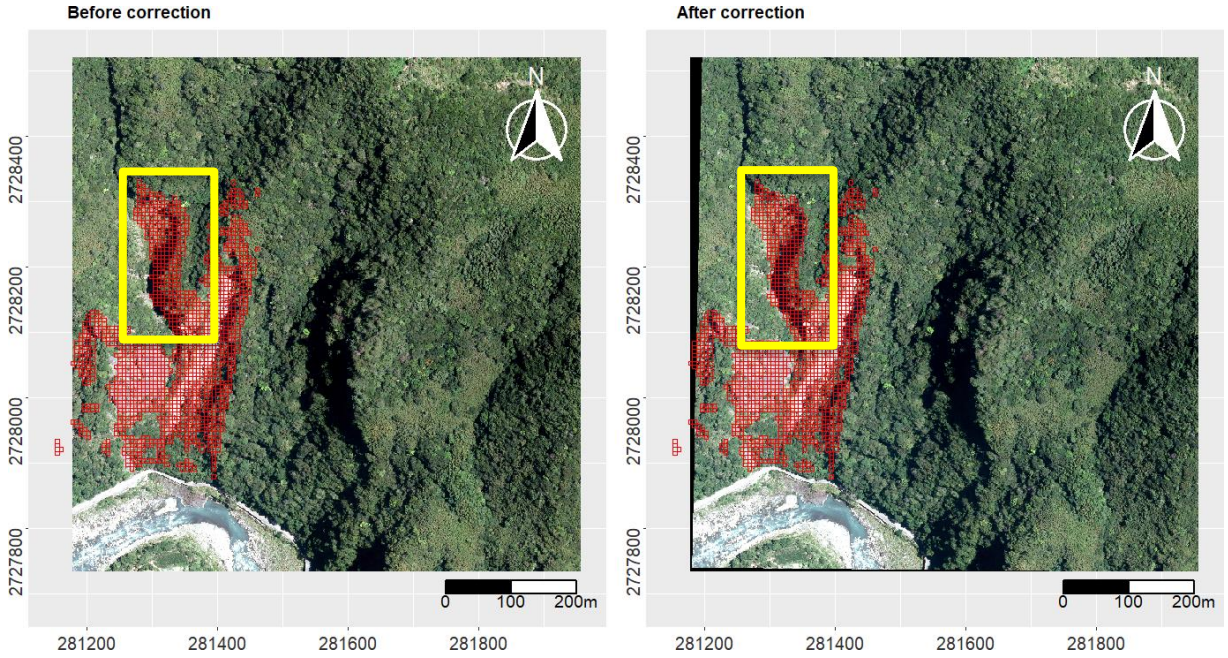

Figure 8 The match between the red squares and the aerial photo improved after a slight rotation

In conclusion, this study established the ranges of monthly NDVI values by calculating the TOA reflectance-based NDVI values of a reference area with year-round vegetation cover. The pixels with NDVI values below the mean NDVI minus three standard deviations were designated as rockfall/rockslide regions of the slope. Images from 2019 to 2021 were studied, and we found that the size of rockfall regions underwent periodic changes. This suggests that

repeated rockfalls occurred on this slope, which local residents confirmed. Therefore, the proposed method of using NDVI to monitor the rockfall behavior of the hillside is feasible. For completeness, Figure 9 displays the rockfall regions found in our analysis for each month of 2021.

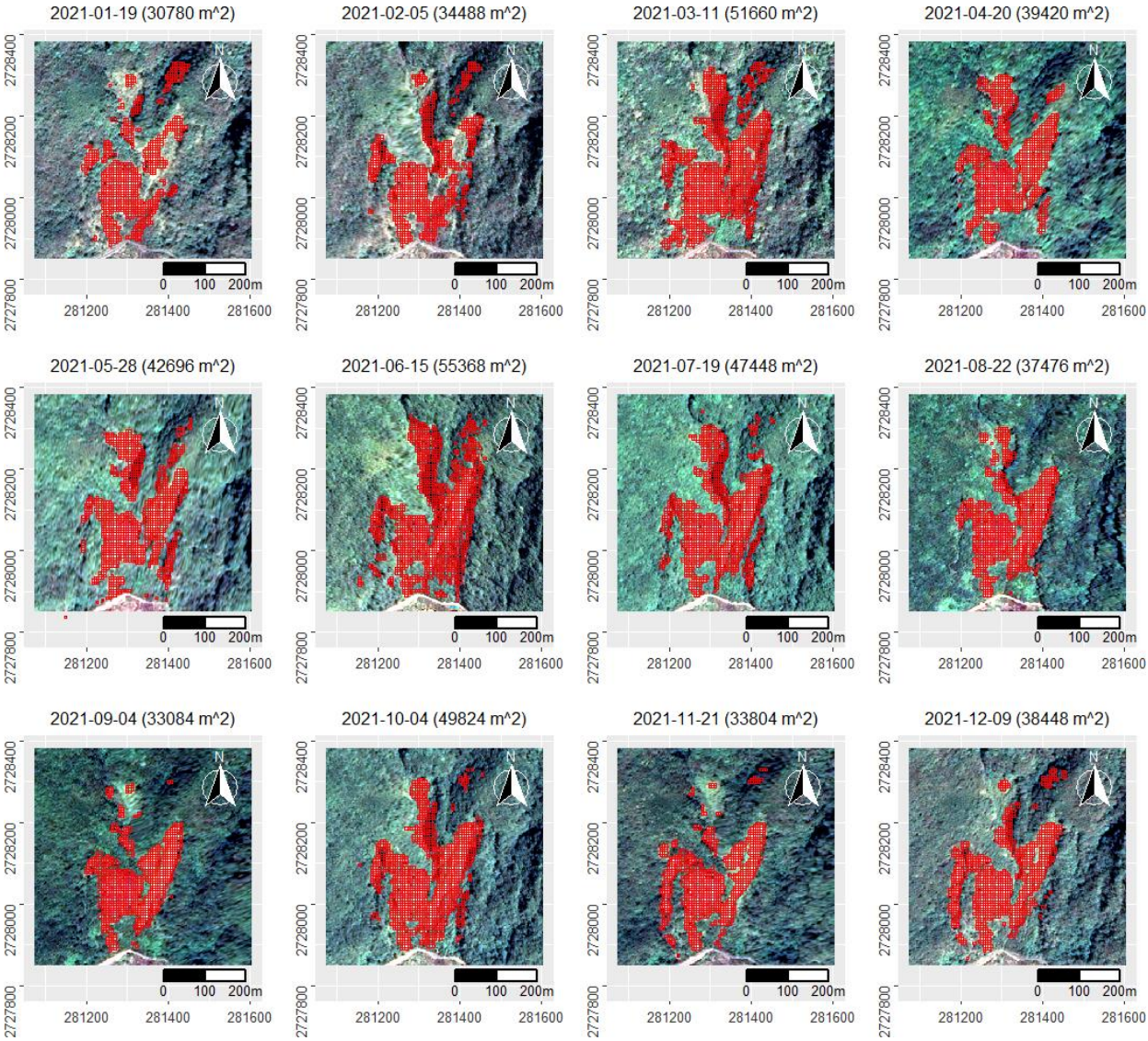

Figure 9 The rockfall regions identified for every month of 2021

References

Astrium Services, 2013. SPOT 6 & SPOT 7 Imagery User Guide. France.

Chao, M. A., Guo, Z. Z., Zhang, X. K., & Han, R. M., 2011. Annual integral changes of time serial NDVI in mining subsidence area. Transactions of Nonferrous Metals Society of China, 21, s583-s588.

Gonzalez Loyarte, M. M., & Menenti, M., 2008. Impact of rainfall anomalies on Fourier parameters of NDVI time series of northwestern Argentina. International Journal of Remote Sensing, 29(4), 1125-1152.

Guerrero, F. J. D. T., Hinojosa-Corona, A., & Kretzschmar, T. G., 2016. A comparative study of NDVI values between north-and south-facing slopes in a semiarid mountainous region. IEEE Journal of Selected Topics in Applied Earth Observations and Remote Sensing, 9(12), 5350-5356.

Kocaaslan, S., Musaoğlu, N., & Karamzadeh, S., 2021. Evaluating Drought Events by Time-Frequency Analysis: A Case Study in Aegean Region of Turkey. IEEE Access, 9, 125032-125041.

Quintano, C., Stein, A., Bijker, W., & Fernandez-Manso, A., 2010. Pattern validation for MODIS image mining of burned area objects. International journal of remote sensing, 31(12), 3065-3087.

Tsai, F., Lai, J. S., Nguyen, K. A., & Chen, W., 2021. Determining Cover Management Factor with Remote Sensing and Spatial Analysis for Improving Long-Term Soil Loss Estimation in Watersheds. ISPRS International Journal of Geo-Information, 10(1), 19.

Tsai, F., Lai, J. S., Chen, W. W., & Lin, T. H., 2013. Analysis of topographic and vegetative factors with data mining for landslide verification. Ecological Engineering, 61, 669-677.

Yang, W., Wang, Y., Sun, S., Wang, Y., & Ma, C., 2019. Using Sentinel-2 time series to detect slope movement before the Jinsha River landslide. Landslides, 16(7), 1313-1324.